ORIGINAL ARTICLE

A C G publications

Org. Commun. XX:X (2025) X-XX

organic communications

Synthesis, molecular docking, and in vitro evaluation of 2,4-dichlorobenzylamide derivatives as soluble epoxide hydrolase (sEH) inhibitors

Kübra Çalışkan[1*], Esra Sadak[1], Paul M. Jordan[2] and Oliver Werz[2]

[1]*Gazi University, Faculty of Pharmacy, Department of Pharmaceutical Chemistry, 06330, Ankara, Türkiye*

[2]*Department of Pharmaceutical/Medicinal Chemistry, Institute of Pharmacy, Friedrich Schiller University Jena, Philosophenweg 14, D-07743, Jena, Germany*

(Received July 28, 2025; Revised August 21, 2025; Accepted August 28, 2025)

Abstract: A novel series of amide-based soluble epoxide hydrolase (sEH) inhibitors was rationally designed by incorporating 2,4-dichlorobenzyl and terminal heterocyclic moieties into a central amide scaffold. The target compounds were synthesized and structurally confirmed as new chemical entities using HRMS, ^{1}H NMR, and ^{13}C NMR spectroscopy. Molecular docking studies of the synthesized inhibitors with sEH revealed key hydrogen bonding interactions with Asp335, Tyr383, and Tyr466, along with π–π stacking interactions with His524 and Trp525, indicating their effective binding to the sEH active site. In vitro biological evaluation showed that all synthesized derivatives exhibit potent sEH inhibitory activity at both 10 and 100 nM, with compound **11** emerging as the most promising lead for further development of potent anti-inflammatory agents.

Keywords: Epoxyeicosatrienoic acids; soluble epoxide hydrolase; heterocyclic compounds; amide-based inhibitors.

1. Introduction

Arachidonic acid (AA) is a 20-carbon polyunsaturated fatty acid that is released from membrane phospholipids upon activation of cytosolic phospholipase A_2 alpha (cPLA$_2$α) in response to inflammatory stimuli.[1] It acts as a crucial precursor in the biosynthesis of a wide range of lipid mediators through three major enzymatic pathways: cyclooxygenase (COX), lipoxygenase (LO), and cytochrome P450 (CYP450). While the COX and LO pathways generate prostaglandins and leukotrienes, the CYP450 pathway leads to the formation of epoxyeicosatrienoic acids (EETs) (Figure 1A).[2, 3]

EETs act as autocrine and paracrine signaling molecules and mediate a wide range of beneficial biological effects, including anti-inflammatory,[4, 5] vasodilatory,[6] cardioprotective,[7] and neuroprotective[8] actions. Through these functions, they play critical roles in key physiological and pathological processes such as cardiovascular regulation,[7] renal function,[9] angiogenesis,[10, 11] nociception,[12] and tumor progression.[13] However, the bioactivity of EETs is tightly regulated by soluble epoxide hydrolase (sEH), an enzyme that hydrolyzes them into more stable but less active diol metabolites, known as dihydroxyeicosatrienoic acids (DHETs) (Figure 1A). This metabolic conversion not only reduces the availability of EETs but also shifts their effects toward a pro-inflammatory profile.[14, 15] Recent studies have associated increased sEH activity, and the resulting reduction in EET levels, with various pathological conditions. Accordingly, the pharmacological inhibition of sEH has emerged as a promising strategy to preserve endogenous EET levels and harness their therapeutic potential in the treatment of

* Corresponding author: E-Mail: kubraibis@gazi.edu.tr

The article was published by ACG Publications
http://www.acgpubs.org/journal/organic-communications © Month-Month 2025 EISSN:1307-6175
DOI: http://doi.org/10.25135/acg.oc.195.2507.3595
Available online: August 31, 2025

various diseases, including neuropathic pain, cancer, and both acute and chronic inflammatory diseases.[16-19]

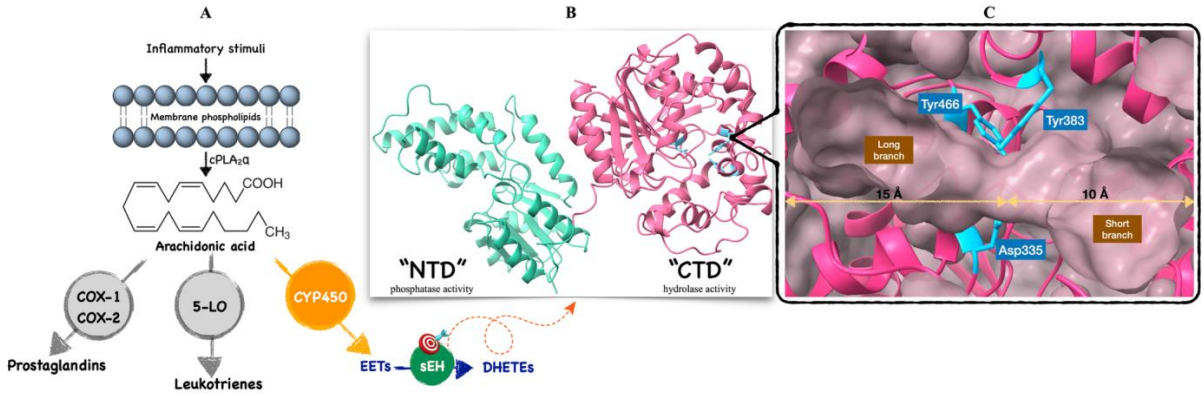

Figure 1. A) Metabolism of AA via COX, 5-LO, and CYP450 pathways into bioactive lipid mediators, highlighting sEH as a potential therapeutic target. **B)** Crystal structure of human sEH (PDB: 3WKE) showing the overall protein conformation. **C)** Location of the hydrolase active site within the CTD.

sEH is ubiquitously expressed in mammalian tissues, with particularly high levels in the liver and kidney. The enzyme comprises two functional domains (Figure 1B): the C-terminal domain (CTD) contains the catalytic center responsible for the hydrolysis of epoxy fatty acids, whereas the N-terminal domain (NTD) exhibits phosphatase activity. However, the biological function of the N-terminal phosphatase domain remains largely unclear.[20, 21] The active site responsible for the hydrolase activity of human sEH, located within the CTD, is embedded in a hydrophobic pocket. This pocket is composed of two branches: a left (long) arm approximately 15 Å in length, and a right (short) arm about 10 Å in length. These two regions are connected by a narrow bottleneck that includes the key catalytic residues Asp335, Tyr383, and Tyr466 (Figure 1C).[22] Such structural features of the active site are critical for understanding inhibitor binding. Indeed, X-ray co-crystal structures reveal that most sEH inhibitors share a central urea or amide pharmacophore, which enables hydrogen bonding with key residues in the catalytic center. This central urea or amide core is flanked by large hydrophobic groups, which interact with the hydrophobic pockets of the active site to enhance inhibitor binding stability.[23, 24] It is suggested that in addition to polar interactions at the catalytic center, hydrophobic and space-filling interactions on both sides of the pocket collectively contribute to the stabilization of ligands within the active site of sEH.[25] In this context, disubstituted urea and amide derivatives have recently emerged as the most promising sEH inhibitors due to their demonstrated antihypertensive, analgesic, anti-inflammatory, and anticancer properties.[4, 16-19] Notably, several of these compounds, such as AR9281, EC5026 and GSK2256294, have progressed into clinical development (Figure 2).[26-28]

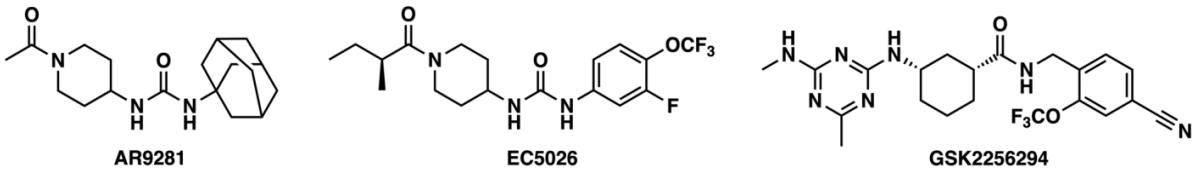

Figure 2. sEH inhibitors in clinical development.

As part of our ongoing efforts to develop novel anti-inflammatory agents, we previously reported a series of potent sEH inhibitors bearing disubstituted urea or amide scaffolds.[29-33] As a continuation of these studies, the present work aimed at designing novel lead compounds based on crystallographic fragment screening data and existing structure-activity relationship (SAR) information on sEH inhibitors. These inhibitors were rationally designed by combining the 2,4-dichlorobenzylamide

pharmacophore — one of the commonly encountered motifs among known sEH inhibitors[34, 35]— with various heterocyclic ring systems inspired by fragment-based screening studies,[23-25] linked through an ether bridge (Figure 3). Thus, we report here our success in identifying new 2,4-dichlorobenzylamide derivatives that potently inhibit sEH and are amenable to further development as potential anti-inflammatory agents.

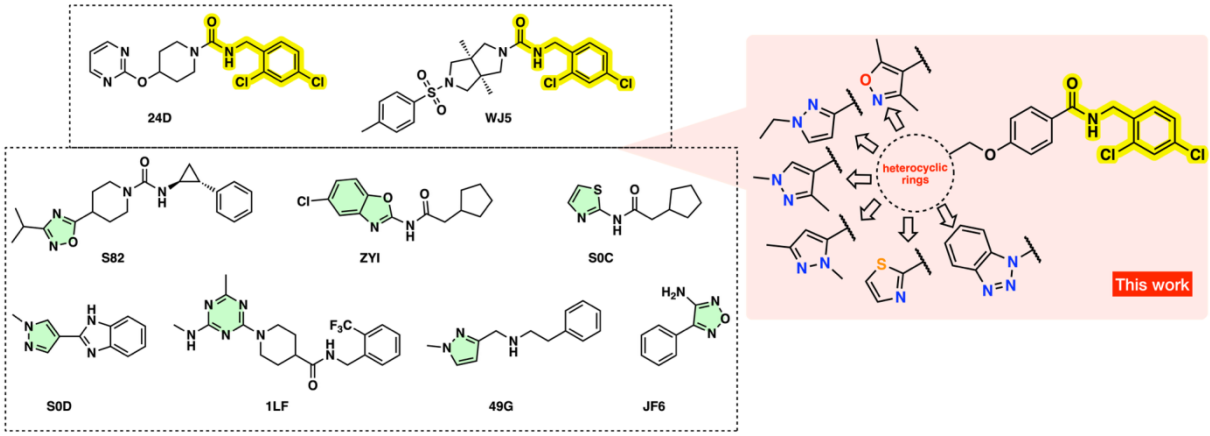

Figure 3. Representative structures of the newly designed 2,4-dichlorobenzylamide derivatives developed in this work, featuring fragment-inspired heterocycles linked to a core pharmacophore via a phenoxy bridge. These fragments (24D, WJ5, S82, ZYI, S0C, S0D, 1LF, 49G, and JF6) are the co-crystallized ligands present in the human sEH PDB crystal structures 3KOO, 8QN0, 3ANT, 3PDC, 3WK5, 3WK7, 4JNC, 4Y2J, and 5AI0, respectively.

2. Experimental

2.1. Chemistry

All chemicals and reagents were purchased from local suppliers. The newly synthesized compounds were purified using a Combiflash® Rf automatic flash chromatography system with RediSep columns (Teledyne-Isco, Lincoln, NE, USA), employing dichloromethane (DCM) and ethyl acetate (EtOAc) gradients. The chemical structures of the compounds were elucidated using ^{1}H NMR and ^{13}C NMR spectra recorded in DMSO-d_6. NMR spectra were recorded on a Bruker Avance Neo 500 MHz spectrometer. Melting points were determined using a Stuart SMP50 melting point apparatus. High-resolution mass spectra (HRMS) were recorded on a Waters LCT Premier XE mass spectrometer operating in ESI(+) mode, coupled to an ultra-performance liquid chromatography (UPLC) system (Waters Corporation, Milford, MA, USA). The purity of all final compounds exceeded 95%, as determined by UPLC with UV detection at 254 nm, using a water/acetonitrile gradient containing 0.1% formic acid (1% → 90%) on an Acquity BEH C18 column (2.1 × 50 mm, 1.7 µm).

2.1.1. Synthesis and Characterization of Intermediates and Final Compounds

*General Procedure for the Synthesis of Intermediates **1-6**:* Methyl 4-hydroxybenzoate (1.0 eq) and K_2CO_3 (1.5 eq) were dissolved in DMF and stirred at room temperature for 30 minutes. Subsequently, the appropriate halide derivative was added, and the reaction mixture was stirred at 80 °C overnight. After completion, the reaction mixture was poured into water, and the resulting precipitate was collected by filtration. Without further purification, the obtained ester derivative was dissolved in a 1:1 mixture of THF and water. LiOH·H_2O (2.5 eq) was added, and the reaction was stirred under reflux at 60 °C for 3 hours. Upon completion, the solvent was evaporated, and water was added to the residue. The aqueous mixture was acidified with concentrated HCl to precipitate the product, which was collected by filtration, dried, and recrystallized from an ethanol-water mixture to afford the pure compound. Spectral data for intermediate compounds 1-6 are provided in the Supporting Information.

*General Procedure for the Synthesis of Final Compounds **7-12***: The corresponding carboxylic acid derivative (1.0 eq) was dissolved in DCM. DMAP (0.2 eq) and 2,4-dichlorobenzylamine (1.1 eq) were added, and the mixture was stirred at room temperature for 15 minutes. Subsequently, EDC·HCl (1.2 eq) was added, and the reaction was allowed to proceed under a nitrogen atmosphere at room temperature overnight. Upon completion, the reaction mixture was extracted with DCM. The combined organic layers were dried over Na_2SO_4, filtered, and concentrated under reduced pressure. The crude product was purified by flash column chromatography using a DCM:ethyl acetate (60:40) mobile phase to afford the pure compound.

*N-(2,4-Dichlorobenzyl)-4-((3,5-dimethylisoxazol-4-yl)methoxy)benzamide (**7**)*: The compound was synthesized starting from compound **1**, following the procedure described above and obtained as a white solid. Yield: 76%; m.p. 180-182 °C. ^{1}H NMR (500 MHz, DMSO-*d*$_6$): δ 8.93 (1H, t, *J* = 5.8 Hz, amide-NH), 7.91 (2H, d, *J* = 8.9 Hz, AA' part of AA'BB' system), 7.61 (1H, d, *J* = 2.1 Hz, 2,4-diCl-Ph-H-3), 7.41 (1H, dd, *J* = 8.4, 2.1 Hz, 2,4-diCl-Ph-H-5), 7.35 (1H, d, *J* = 8.4 Hz, 2,4-diCl-Ph-H-6), 7.10 (2H, d, *J* = 8.9 Hz, BB' part of AA'BB' system), 5.00 (2H, s, -O-C$\underline{H}_2$-), 4.50 (2H, d, *J* = 5.8 Hz, -NH-C$\underline{H}_2$-), 2.42 (3H, s, -C$\underline{H}_3$), 2.22 (3H, s, -C$\underline{H}_3$). ^{13}C NMR (125 MHz, DMSO-*d*$_6$): δ 168.00, 166.34, 161.09, 160.00, 136.30, 133.31, 132.56, 130.49, 129.63, 129.01, 127.78, 127.05, 114.99, 110.64, 59.64, 40.63, 11.13, 10.19. HRMS (ESI) *m/z:* $[M+H]^+$ calcd for $C_{20}H_{19}Cl_2N_2O_3$, 405.0773; found, 405.0764.

*N-(2,4-Dichlorobenzyl)-4-((1-ethyl-1H-pyrazol-3-yl)methoxy)benzamide (**8**)*: The compound was synthesized starting from compound **2**, following the procedure described above and obtained as a white solid. Yield: 71%; m.p. 136-137 °C. ^{1}H NMR (500 MHz, DMSO-*d*$_6$): δ 8.91 (1H, t, *J* = 5.8 Hz, amide-NH), 7.87 (2H, d, *J* = 8.9 Hz, AA' part of AA'BB' system), 7.71 (1H, d, *J* = 2.2 Hz, Pyrazole-H-4), 7.61 (1H, d, *J* = 2.1 Hz, 2,4-diCl-Ph-H-3), 7.41 (1H, dd, *J* = 8.4, 2.1 Hz, 2,4-diCl-Ph-H-5), 7.34 (2H, d, *J* = 8.4 Hz, 2,4-diCl-Ph-H-6), 7.10 (2H, d, *J* = 8.9 Hz, BB' part of AA'BB' system), 6.31 (1H, d, *J* = 2.2 Hz, Pyrazole-H-5), 5.07 (2H, s, -O-C$\underline{H}_2$-), 4.48 (2H, d, *J* = 5.8 Hz, -NH-C$\underline{H}_2$-), 4.12 (2H, q, *J* = 7.2 Hz, CH$_3$-C$\underline{H}_2$-pyrazole), 1.36 (3H, t, *J* = 7.2 Hz, C$\underline{H}_3$-CH$_2$-pyrazole). ^{13}C NMR (125 MHz, DMSO-*d*$_6$): δ 166.40, 161.33, 147.13, 136.32, 133.27, 132.53, 130.70, 130.47, 129.58, 128.99, 127.79, 126.68, 114.76, 105.59, 64.26, 46.62, 40.61, 15.97. HRMS (ESI) *m/z:* $[M+H]^+$ calcd for $C_{20}H_{20}Cl_2N_3O_2$, 404.0933; found, 404.0925.

*N-(2,4-Dichlorobenzyl)-4-((1,3-dimethyl-1H-pyrazol-4-yl)methoxy)benzamide (**9**)*: The compound was synthesized starting from compound **3**, following the procedure described above and obtained as a white solid. Yield: 87%; m.p. 174-176 °C. ^{1}H NMR (500 MHz, DMSO-*d*$_6$): δ 8.91 (1H, t, *J* = 5.8 Hz, amide-NH), 7.88 (2H, d, *J* = 9.0 Hz, AA' part of AA'BB' system), 7.69 (1H, br s, Pyrazole-H), 7.60 (1H, d, *J* = 2.2 Hz, 2,4-diCl-Ph-H-3), 7.41 (1H, dd, *J* = 8.4, 2.2 Hz, 2,4-diCl-Ph-H-4), 7.34 (1H, d, *J* = 8.4 Hz, 2,4-diCl-Ph-H-5), 7.06 (2H, d, *J* = 9.0 Hz, BB' part of AA'BB' system), 4.96 (2H, s, -O-C$\underline{H}_2$-), 4.49 (2H, d, *J* = 5.8 Hz, -NH-C$\underline{H}_2$-), 3.73 (3H, s, -C$\underline{H}_3$), 2.15 (3H, s, -C$\underline{H}_3$). ^{13}C NMR (125 MHz, DMSO-*d*$_6$): δ 166.41, 161.38, 146.97, 136.33, 133.28, 132.53, 132.06, 130.46, 129.58, 128.99, 127.77, 126.54, 114.83, 114.11, 61.11, 40.61, 38.61, 11.85. HRMS (ESI) *m/z*: $[M+H]^+$ calcd for $C_{20}H_{20}Cl_2N_3O_2$, 404.0933; found, 404.0939.

*N-(2,4-Dichlorobenzyl)-4-((1,3-dimethyl-1H-pyrazol-5-yl)methoxy)benzamide (**10**)*: The compound was synthesized starting from compound **4**, following the procedure described above and obtained as a white solid. Yield: 89%; m.p. 152-153 °C. ^{1}H NMR (500 MHz, DMSO-*d*$_6$): δ 8.94 (1H, t, *J* = 5.8 Hz, amide-NH), 7.90 (2H, d, *J* = 8.9 Hz, AA' part of AA'BB' system), 7.61 (1H, d, *J* = 2.1 Hz, 2,4-diCl-Ph-H-3), 7.41 (1H, dd, *J* = 8.4, 2.1 Hz, 2,4-diCl-Ph-H-5), 7.35 (1H, d, *J* = 8.4 Hz, 2,4-diCl-Ph-H-6), 7.12 (2H, d, *J* = 8.9 Hz, BB' part of AA'BB' system), 6.16 (1H, s, Pyrazole-H), 5.19 (2H, s, -O-C$\underline{H}_2$-), 4.50 (2H, d, *J* = 5.8 Hz, -NH-C$\underline{H}_2$-), 3.75 (3H, s, -C$\underline{H}_3$), 2.12 (3H, s, -C$\underline{H}_3$). ^{13}C NMR (125 MHz, DMSO-*d*$_6$): δ 166.32, 160.78, 146.06, 138.12, 136.28, 133.30, 132.55, 130.48, 129.62, 129.00, 127.78, 127.12, 114.95, 107.04, 60.58, 40.62, 36.55, 13.62. HRMS (ESI) m/z: $[M+H]^+$ calcd for $C_{20}H_{20}Cl_2N_3O_2$, 404.0933; found, 404.0952.

*N-(2,4-Dichlorobenzyl)-4-(thiazol-2-ylmethoxy)benzamide (**11**)*: The compound was synthesized starting from compound **5**, following the procedure described above and obtained as a white solid. Yield: 80%; m.p. 136-137 °C. ^{1}H NMR (500 MHz, DMSO-*d*$_6$): δ 8.95 (1H, t, *J* = 5.8 Hz, amide-NH), 7.91 (2H, d, *J* = 8.8 Hz, AA' part of AA'BB' system), 7.86 (1H, d, *J* = 3.3 Hz, Thiazole-H-4), 7.79 (1H, d, *J* = 3.3 Hz, Thiazole-H-5), 7.60 (1H, d, *J* = 2.1 Hz, 2,4-diCl-Ph-H-3), 7.41 (1H, dd, *J* = 8.3, 2.1 Hz, 2,4-diCl-Ph-H-5), 7.35 (1H, d, *J* = 8.3 Hz, 2,4-diCl-Ph-H-6), 7.16 (2H, d, *J* = 8.8 Hz, BB' part of AA'BB' system), 5.53 (2H, s, -O-C$\underline{H}_2$-), 4.50 (2H, d, *J* = 5.8 Hz, -NH-C$\underline{H}_2$-). ^{13}C NMR (125 MHz, DMSO-*d*$_6$): δ 166.29, 166.09, 160.47, 143.10, 136.25, 133.30, 132.56, 130.49, 129.70, 128.99, 127.78, 127.51, 121.74, 115.04, 67.07, 40.63. HRMS (ESI) *m/z:* $[M+H]^+$ calcd for $C_{18}H_{15}Cl_2N_2O_2S$, 393.0231; found, 393.0228.

*4-((1H-benzo[d][1,2,3]triazol-1-yl)methoxy)-N-(2,4-dichlorobenzyl)benzamide (**12**)*: The compound was synthesized starting from compound **6**, following the procedure described above and obtained as a white solid. Yield: 68%; m.p. 189-191 °C. ^{1}H NMR (500 MHz, DMSO-*d*$_6$): δ 8.96 (1H, t, *J* = 5.8 Hz, amide NH), 8.10 (1H, d, *J* = 8.0 Hz, Benzotriazole-H-4), 7.99 (2H, d, *J* = 8.0 Hz, Benzotriazole-H-7), 7.89 (2H, d, *J* = 8.9 Hz, AA' part of AA'BB' system), 7.64 (1H, t, *J* = 8.0 Hz, Benzotriazole-H-6), 7.60 (1H, d, *J* = 2.1 Hz, 2,4-diCl-Ph-H-3), 7.47 (1H, t, *J* = 8.0, Benzotriazole-H-5), 7.39 (1H, dd, *J* = 8.4, 2.1 Hz, 2,4-diCl-Ph-H-5), 7.34 (1H, d, *J* = 8.4 Hz, 2,4-diCl-Ph-H-6), 7.27 (2H, d, *J* = 8.9 Hz, BB' part of AA'BB' system), 6.88 (2H, s, -O-C$\underline{H}_2$-), 4.49 (2H, d, *J* = 5.8 Hz, -NH-C$\underline{H}_2$-). ^{13}C NMR (125 MHz, DMSO-*d*$_6$): δ 166.16, 158.73, 145.78, 136.16, 133.30, 133.16, 132.57, 130.50, 129.69, 128.99, 128.84, 128.55, 127.78, 125.16, 119.90, 116.18, 111.18, 74.11, 40.64. HRMS (ESI) *m/z:* $[M+H]^+$ calcd for $C_{21}H_{17}Cl_2N_4O_2$, 427.0729; found, 427.0734.

2.2. Biological Activity

Human recombinant sEH was expressed and purified according to previously established protocols.[36] Briefly, Sf9 insect cells were infected with a recombinant baculovirus (generously provided by Dr. Bruce Hammock, University of California, Davis, CA). Seventy-two hours post-infection, the cells were harvested by centrifugation and lysed via sonication (3 × 10 s at 4 °C) in a lysis buffer containing 10% glycerol, 50 mM NaH_2PO_4 (pH 8.0), 10 µg/mL leupeptin, 300 mM NaCl, 1 mM phenylmethanesulfonyl fluoride (PMSF), 1 mM EDTA, and 60 µg/mL soybean trypsin inhibitor. The resulting lysate was centrifuged at 100,000 × g for 60 minutes at 4 °C, and the supernatant was purified by benzylthiosepharose-affinity chromatography. Elution was performed using 4-fluorochalcone oxide in PBS supplemented with 1 mM DTT and 1 mM EDTA. The purified enzyme was dialyzed, concentrated using a Millipore Amicon Ultra-15 centrifugal filter unit, and quantified for total protein content using a commercial protein assay kit (Bio-Rad Laboratories, Munich, Germany).

The epoxide hydrolase activity of sEH was evaluated using a fluorescence-based assay, as described previously.[37] The enzyme was diluted in 25 mM Tris buffer (pH 7.0) containing 0.1 mg/mL bovine serum albumin (BSA) to an appropriate concentration and preincubated with either test compounds or 0.1% DMSO (vehicle control) for 10 minutes at room temperature. The reaction was initiated by the addition of 50 µM PHOME (3-phenyl-cyano(6-methoxy-2-naphthalenyl)methyl ester-2-oxiraneacetic acid), a non-fluorescent substrate enzymatically converted by sEH into fluorescent 6-methoxy-naphthaldehyde. After 60 minutes of incubation, the reaction was terminated by the addition of 200 mM $ZnSO_4$. Fluorescence was then measured at (λ_{em} 465 nm, λ_{ex} 330 nm) using a NOVOstar microplate reader (BMG LABTECH GmbH, Ortenberg, Germany). When necessary, background fluorescence originating from test compounds was subtracted from the fluorescence signal.

2.3. Molecular Modeling

Molecular docking simulations were performed to investigate the potential binding mode of target compounds within the hydrolase domain of sEH. The recently resolved crystal structure of human sEH in complex with a bound ligand (PDB ID: 8QN0, 1.49 Å resolution) was retrieved from the RCSB Protein Data Bank and selected as the target due to its high structural quality.[35] Protein preparation was carried out using Schrödinger's Protein Preparation Wizard (Maestro Version 7.0.136, Release 2025-2). Missing side chains were added, bond orders were assigned, and protonation states were adjusted to physiological pH (7.4 ± 2.0). Solvent molecules present in the crystal structure were retained throughout

the simulations. The OPLS4 force field was used for all molecular mechanics-based calculations. The ligands were prepared using the LigPrep module, where their ionization states and tautomers were generated at pH 7.4 ± 2.0. Docking grids were generated using Glide, centered on the co-crystal ligand (hereafter referred to as the co-ligand) with a box size extending 10 Å from the centroid. The van der Waals radius scaling factors were set to 0.80 for ligands and 0.25 for the receptor, while the partial charge cutoff was set to 1.0. The co-ligand was first removed and then re-docked into the active site using Glide in Standard Precision (SP) mode. The resulting pose exhibited a root-mean-square deviation (RMSD) of 0.39 Å, confirming the reliability of the docking protocol. Visualization of docking poses and preparation of molecular graphics were performed using ChimeraX (version 1.10).

3. Results and Discussion

3.1. Chemistry

The synthetic route for the compounds is illustrated in Scheme 1. Compounds **1-6** were synthesized from methyl 4-hydroxybenzoate through a two-step synthetic procedure. In the first step, alkylation was carried out at 80 °C in DMF using various halide derivatives bearing five-membered or fused heterocyclic rings containing nitrogen or oxygen atoms at different positions, in the presence of K_2CO_3. The resulting ester-containing intermediates were directly hydrolyzed, without further purification, using $LiOH{\cdot}H_2O$ in a 1:1 THF:H_2O mixture at 60 °C for approximately 3 hours, affording the corresponding carboxylic acid derivatives (**1-6**). These intermediates were subsequently coupled with 2,4-dichlorobenzylamine in the presence of EDC·HCl and DMAP in DCM at room temperature to yield the target amide derivatives (**7-12**). All reactions were conducted in accordance with procedures previously reported in the literature.[32, 38]

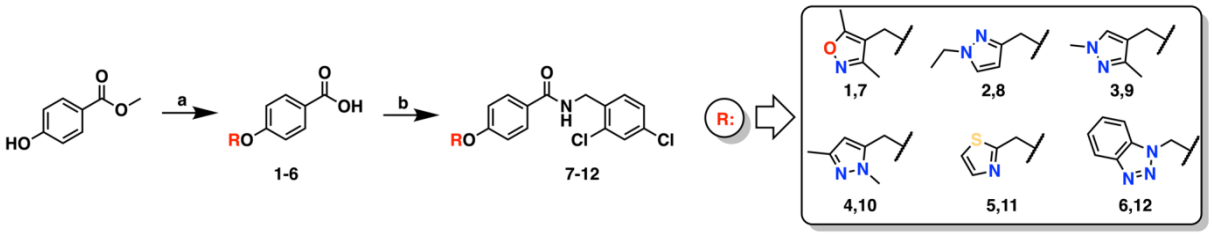

Scheme 1. Synthetic route of the final compounds **7–12**. Reagents and conditions: a) i. Appropriate halide derivatives, K_2CO_3, DMF, 80 °C, overnight; ii. $LiOH{\cdot}H_2O$, THF:H_2O, 60 °C, 3h then 5 M HCl (pH=3) b) 2,4-Dichlorobenzylamine, EDC·HCl, DMAP, DCM, rt, overnight.

The chemical structures of both the intermediates and the final compounds were confirmed by HRMS, ^{1}H NMR, and/or ^{13}C NMR analyses. The corresponding spectral figures for the final compounds are available in the Supporting Information.

3.2. Biological Activity

It should be emphasized that the current study was designed as a preliminary screening to identify promising compounds rather than to establish precise IC_{50} values. Therefore, inhibitory effects of the target compounds against human recombinant sEH were evaluated at 100, 10, and 1 nM, and the percentage of remaining enzyme activity is presented in Figure 4. The results demonstrate a clear concentration-dependent inhibition profile across the tested compounds. At 100 nM, all compounds significantly inhibited sEH activity, with compound **11** showing the most potent effect, reducing residual enzymatic activity to 8.2% (~92% inhibition). Compounds **7-10** and **12** also exhibited potent inhibitory effects at 100 nM with remaining sEH activity in the range of 15.3 to 21.5%. At 10 nM, sEH inhibitory activity decreased across the series; yet compound **9** and **11** continued to demonstrate notable inhibition, with 55.3 and 50.8% residual activities, outperforming all other compounds. At the 1 nM level, however, most compounds failed in inhibitory efficiency. At 1 nM, most compounds showed weak inhibition, and in a few cases, apparent “activation” relative to the control was observed. We attribute this effect to

experimental variability at low concentrations, where the inhibition is close to the detection limit of the assay. Such deviations are within the expected error margin and do not indicate true enzymatic activation. Based on the present results, compound **11**, and to a lesser extent compounds **9**, **10**, and **12**, have been identified as promising leads and will be subjected to full IC_{50} determination and further biological evaluation in future studies. In summary, compound **11** is identified as the most promising candidate within this series, as it displayed consistent and potent sEH inhibition at both 10 and 100 nM, and may serve as a valuable lead for further optimization.

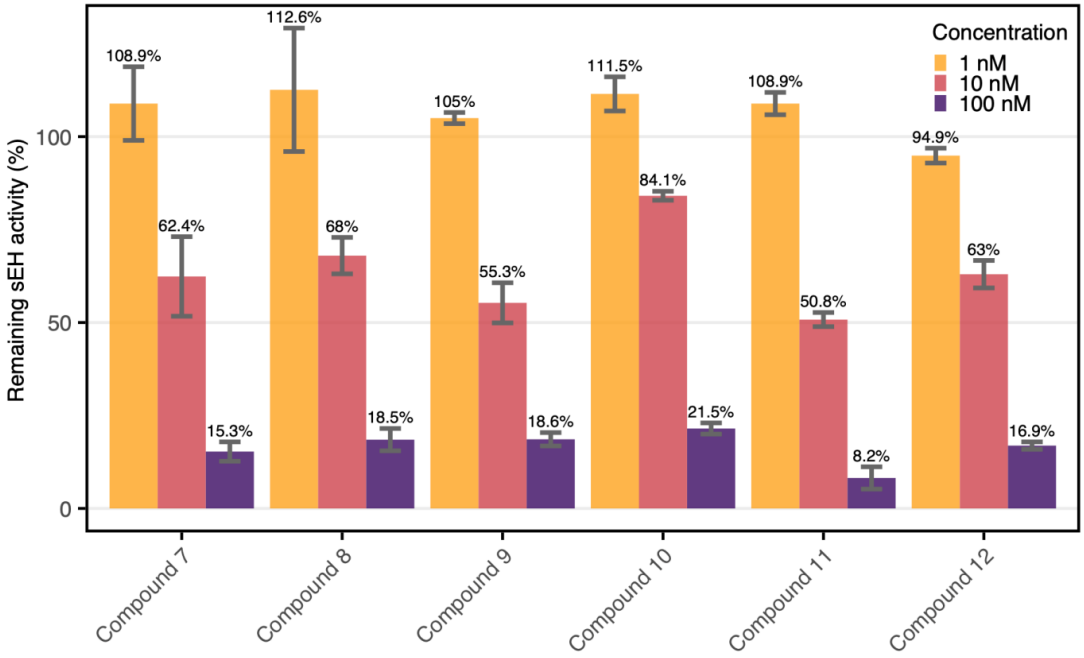

Figure 4. Remaining sEH activity (%) in the presence of final compounds at various concentrations. Results are presented as the mean ± standard error of the mean (SEM) of three independent measurements (n = 3) and expressed as the percentage of residual enzymatic activity relative to the control group (100%, vehicle-treated, uninhibited control).

3.3. Molecular Modeling

To investigate the binding interactions of the target compounds within the active site of sEH, molecular docking studies were performed using the recently resolved crystal structure (PDB ID: 8QN0). The docking protocol was validated by re-docking the co-ligand (Figure 5A), which reproduced the experimental binding pose with a RMSD of 0.39 Å, confirming the reliability of the docking setup (Figure 5B and 5C).

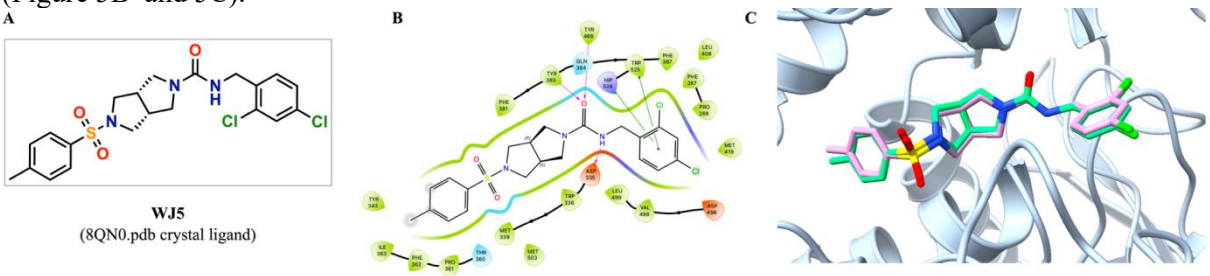

Figure 5. A) Chemical structure of the co-ligand in PDB ID: 8QN0. **B)** 2D interaction diagram showing key contacts between the co-ligand and surrounding active site residues. **C)** Superimposition of the original (pink) and re-docked (green) poses of the co-ligand in the sEH active site.

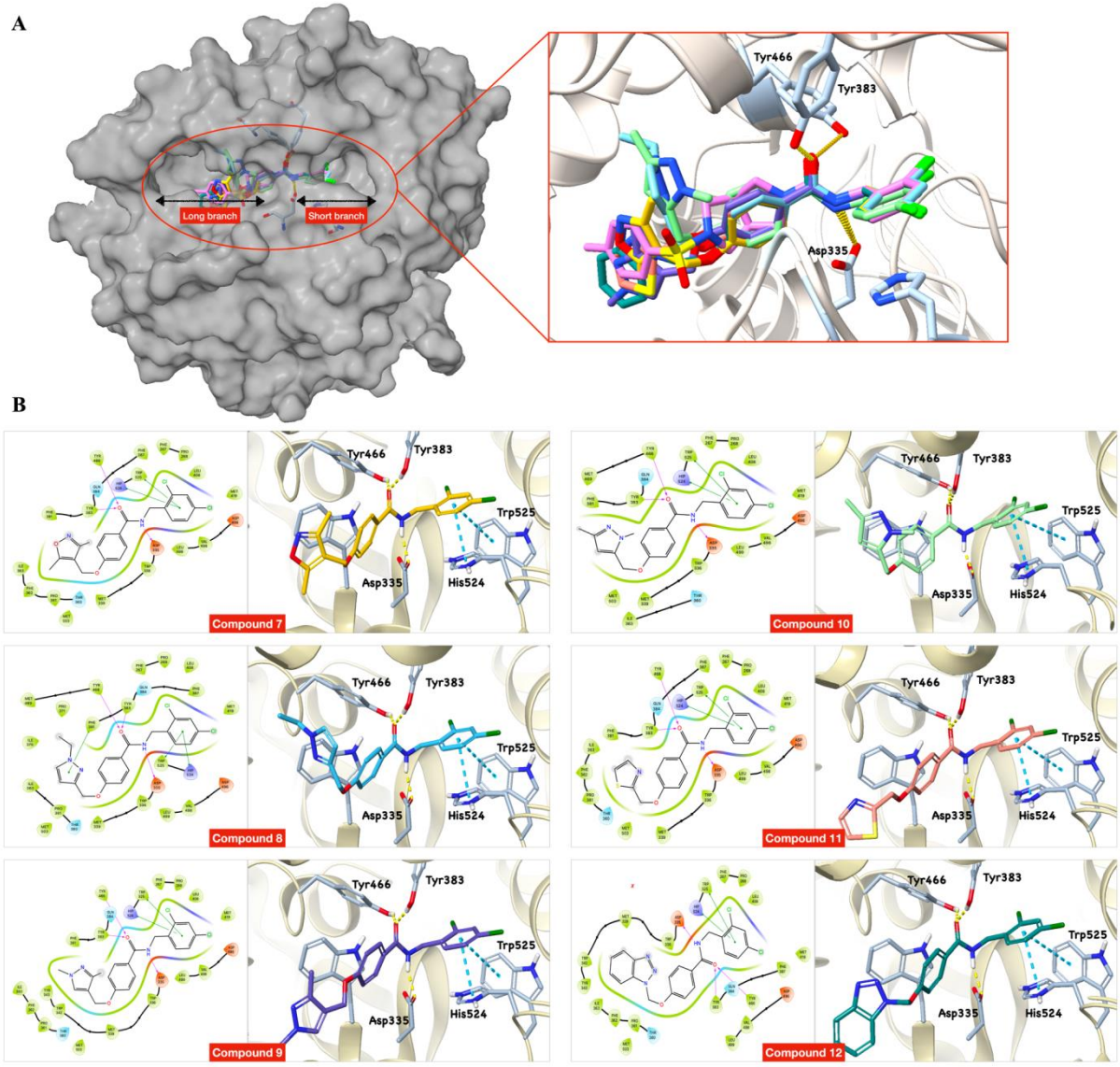

Figure 6. (A) Alignment of the final compounds with the co-ligand in the sEH active site. **(B)** 2D ligand interaction diagram and 3D docking poses of the final compounds. (The co-ligand is shown in pink. Compounds **7, 8, 9, 10, 11**, and **12** are represented in yellow, blue, purple, light green, orange, and dark green, respectively. Hydrogen bonds are shown in yellow, and π–π interactions are indicated in blue.)

Following this validation, the same parameters were applied to explore the binding modes of the target compounds. Initially, all compounds were aligned within the active site in the presence of the co-ligand from the crystal structure. As shown in Figure 6A, the 2,4-dichlorobenzylamide moiety, present in all final compounds as well as in the co-ligand, shows perfect overlap, indicating a conserved binding mode. Figure 6B displays both the 2D and 3D docking poses of the final compounds. As illustrated, all compounds interact with the catalytic center via their amide groups and are positioned within the narrow channel of the active site, in a manner similar to previously reported amide-type sEH inhibitors. Specifically, the carbonyl oxygen forms hydrogen bonds with Tyr383 and Tyr466, while the amide NH group establishes an H-bond with Asp335. Moreover, the 2,4-dichlorobenzyl moieties of the compounds occupy the right-side hydrophobic pocket, analogous to the co-ligand in the crystal structure, and engage in π-π stacking interactions with His524 and Trp525. The heterocyclic ring systems of the compounds extend into the left hydrophobic pocket, filling the van der Waals volume surrounded by key hydrophobic residues such as Pro361, Phe362, Ile363, and Phe381. The docking scores and MM-

GBSA ΔG binding free energies of the compounds are presented in Table 1. Overall, these results indicate favorable binding energies towards sEH.

Table 1. Docking scores and MM-GBSA ΔG binding free energies of the compounds against sEH.

Compound	Glide GScore (kcal/mol)	MM-GBSA ΔG binding free energy (kcal/mol)
7	-11.192	-108.15
8	-11.329	-109.06
9	-10.042	-108.02
10	-11.184	-96.99
11	-11.063	-110.12
12	-12.059	-105.44

4. Conclusion

The revealed structural features of various sEH inhibitor classes suggest that these compounds anchor to the enzyme's active site primarily through urea or amide groups, forming strong hydrogen bonds with key catalytic residues located at the bottleneck of the binding pocket. Additionally, pendant groups attached to the amide/urea cores are known to stabilize binding via hydrophobic and van der Waals interactions. Fragment-based X-ray crystallographic screening studies have further demonstrated that diverse heteroaryl fragments can occupy the left hydrophobic sub-pocket, while right-side sub-pockets are well-accommodated by -CF_3, -CN, or -Cl substituted benzyl groups.[23, 24] Based on these insights, we designed a novel series of sEH inhibitors by decorating the central amide core with a 2,4-dichlorobenzyl group on the right side and various heterocyclic moieties connected through a phenoxy linker on the left. Molecular modeling studies confirmed that the target compounds adopt similar binding modes to reported amide-type sEH inhibitors, forming stable hydrogen bonds with the key residues Asp335, Tyr383, and Tyr466. Furthermore, the 2,4-dichlorobenzyl moiety of the compounds engaged in π-π interactions with His524 and Trp525 within the right hydrophobic pocket, while the phenoxy-linked heterocycles effectively occupied the left pocket, filling the available van der Waals volume. Biological evaluation against human recombinant sEH revealed that the target compounds exhibited moderate to potent inhibitory activity, particularly at concentrations of 100 nM and 10 nM. Among them, compound **11** demonstrated the most promising inhibitory profile across the series, suggesting its potential as a valuable lead for the development of more potent and selective sEH inhibitors.

Acknowledgements

This study was supported by the TÜBİTAK 2209-A Research Project (Application No. 1919B012323990) and by the Deutsche Forschungsgemeinschaft (DFG), SFB 1278 "PolyTarget" (project number 316213987, projects A04) and SFB1127 "ChemBioSys" (project number 239748522, project A04). The authors sincerely thank Prof. Dr. Erden Banoğlu and Prof. Dr. Burcu Çalışkan of Gazi University for their and critical reading of the manuscript.

Supporting Information

Supporting information accompanies this paper on http://www.acgpubs.org/journal/organic-communications

ORCID
Kübra Çalışkan: 0000-0002-6898-0258
Esra Sadak: 0009-0008-8675-5522
Paul M. Jordan: 0000-0002-8364-4236
Oliver Werz: 0000-0002-5064-4379

References

[1] Meirer, K.; Steinhilber, D.; Proschak, E. Inhibitors of the arachidonic acid cascade: interfering with multiple pathways. *Basic Clin. Pharmacol. Toxicol.* **2014**, *114*, 83–91.

[2] Kroetz, D. L.; Zeldin, D. C. Cytochrome P450 pathways of arachidonic acid metabolism. *Curr. Opin. Lipidol.* **2002**, *13*, 273–283.

[3] Wang, B.; Wu, L.; Chen, J.; Dong, L.; Chen, C.; Wen, Z.; Hu, J.; Fleming, I.; Wang, D. W. Metabolism pathways of arachidonic acids: mechanisms and potential therapeutic targets. *Sig. Transduct. Target Ther.* **2021**, *6*, 94.

[4] Shi, Z.; He, Z.; Wang, D. W. CYP450 Epoxygenase Metabolites, Epoxyeicosatrienoic Acids, as Novel Anti-Inflammatory Mediators. *Molecules* **2022**, *27*, 3873.

[5] Thomson, S. J.; Askari, A.; Bishop-Bailey, D. Anti-inflammatory effects of epoxyeicosatrienoic acids. *Int. J. Vasc. Med.* **2012**, *2012*, 605101.

[6] Pfister, S. L.; Gauthier, K. M.; Campbell, W. B. Chapter 2 - Vascular Pharmacology of Epoxyeicosatrienoic Acids. In *Advances in Pharmacology*, Vanhoutte, P. M. Ed., Vol. 60, 2010, p. 27.

[7] Yang, L.; Maki-Petaja, K.; Cheriyan, J.; McEniery, C.; Wilkinson, I. B. The role of epoxyeicosatrienoic acids in the cardiovascular system. *Br. J. Clin. Pharmacol.* **2015**, *80*, 28–44.

[8] Wang, L.; Luo, G.; Zhang, L. F.; Geng, H. X. Neuroprotective effects of epoxyeicosatrienoic acids. *Prostaglandins Other Lipid Mediat.* **2018**, *138*, 9–14.

[9] Schragenheim, J.; Bellner, L.; Cao, J.; Singh, S. P.; Bamshad, D.; McClung, J. A.; Maayan, O.; Meissner, A.; Grant, I.; Stier, C. T.; et al. EET enhances renal function in obese mice resulting in restoration of HO-1-Mfn1/2 signaling, and decrease in hypertension through inhibition of sodium chloride co-transporter. *Prostaglandins Other Lipid Mediat.* **2018**, *137*, 30–39.

[10] Fleming, I. Epoxyeicosatrienoic acids, cell signaling and angiogenesis. *Prostaglandins Other Lipid Mediat.* **2007**, *82*, 60–67.

[11] Michaelis, U. R.; Fleming, I. From endothelium-derived hyperpolarizing factor (EDHF) to angiogenesis: Epoxyeicosatrienoic acids (EETs) and cell signaling. *Pharmacol. Ther.* **2006**, *111*, 584–595.

[12] Turnbull, J.; Chapman, V. Targeting the soluble epoxide hydrolase pathway as a novel therapeutic approach for the treatment of pain. *Curr. Opin. Pharmacol.* **2024**, *78*, 102477.

[13] Panigrahy, D.; Edin, M. L.; Lee, C. R.; Huang, S.; Bielenberg, D. R.; Butterfield, C. E.; Barnes, C. M.; Mammoto, A.; Mammoto, T.; Luria, A.; et al. Epoxyeicosanoids stimulate multiorgan metastasis and tumor dormancy escape in mice. *J. Clin. Invest.* **2012**, *122*, 178–191.

[14] Spector, A. A.; Fang, X.; Snyder, G. D.; Weintraub, N. L. Epoxyeicosatrienoic acids (EETs): metabolism and biochemical function. *Prog. Lipid Res.* **2004**, *43*, 55–90.

[15] Spector, A. A.; Kim, H. Y. Cytochrome P450 epoxygenase pathway of polyunsaturated fatty acid metabolism. *Biochim. Biophys. Acta.* **2015**, *1851*, 356–365.

[16] Kelly, A. G.; Wang, W.; Rothenberger, E.; Yang, J.; Gilligan, M. M.; Kipper, F. C.; Attaya, A.; Gartung, A.; Hwang, S. H.; Gillespie, M. J.; et al. Enhancing cancer immunotherapy via inhibition of soluble epoxide hydrolase. *Proc. Natl. Acad. Sci. U. S. A.* **2024**, *121*, e2314085121.

[17] Pillarisetti, S.; Khanna, I. A multimodal disease modifying approach to treat neuropathic pain--inhibition of soluble epoxide hydrolase (sEH). *Drug Discov. Today.* **2015**, *20*, 1382–1390.

[18] Schmelzer, K. R.; Kubala, L.; Newman, J. W.; Kim, I. H.; Eiserich, J. P.; Hammock, B. D. Soluble epoxide hydrolase is a therapeutic target for acute inflammation. *Proc. Natl. Acad. Sci. U. S. A.* **2005**, *102*, 9772–9777.

[19] Wagner, K. M.; McReynolds, C. B.; Schmidt, W. K.; Hammock, B. D. Soluble epoxide hydrolase as a therapeutic target for pain, inflammatory and neurodegenerative diseases. *Pharmacol. Ther.* **2017**, *180*, 62–76.

[20] Hiesinger, K.; Wagner, K. M.; Hammock, B. D.; Proschak, E.; Hwang, S. H. Development of multitarget agents possessing soluble epoxide hydrolase inhibitory activity. *Prostaglandins Other Lipid Mediat.* **2019**, *140*, 31–39.

[21] Kramer, J.; Proschak, E. Phosphatase activity of soluble epoxide hydrolase. *Prostaglandins Other Lipid Mediat.* **2017**, *133*, 88–92.

[22] Gomez, G. A.; Morisseau, C.; Hammock, B. D.; Christianson, D. W. Structure of human epoxide hydrolase reveals mechanistic inferences on bifunctional catalysis in epoxide and phosphate ester hydrolysis. *Biochemistry.* **2004**, *43*, 4716–4723.

[23] Amano, Y.; Tanabe, E.; Yamaguchi, T. Identification of N-ethylmethylamine as a novel scaffold for inhibitors of soluble epoxide hydrolase by crystallographic fragment screening. *Bioorg. Med. Chem.* **2015**, *23*, 2310–2317.

[24] Amano, Y.; Yamaguchi, T.; Tanabe, E. Structural insights into binding of inhibitors to soluble epoxide hydrolase gained by fragment screening and X-ray crystallography. *Bioorg. Med. Chem.* **2014**, *22*, 2427–2434.

[25] Bzowka, M.; Mitusinska, K.; Hopko, K.; Gora, A. Computational insights into the known inhibitors of human soluble epoxide hydrolase. *Drug Discov Today.* **2021**, *26*, 1914–1921.

[26] Anandan, S. K.; Webb, H. K.; Chen, D.; Wang, Y. X.; Aavula, B. R.; Cases, S.; Cheng, Y.; Do, Z. N.; Mehra, U.; Vinh, T.; et al. 1-(1-Acetyl-piperidin-4-yl)-3-adamantan-1-yl-urea (AR9281) as a potent, selective, and orally available soluble epoxide hydrolase inhibitor with efficacy in rodent models of hypertension and dysglycemia. *Bioorg. Med. Chem. Lett.* **2011**, *21*, 983–988.

[27] Hammock, B. D.; McReynolds, C. B.; Wagner, K.; Buckpitt, A.; Cortes-Puch, I.; Croston, G.; Lee, K. S. S.; Yang, J.; Schmidt, W. K.; Hwang, S. H. Movement to the Clinic of Soluble Epoxide Hydrolase Inhibitor EC5026 as an Analgesic for Neuropathic Pain and for Use as a Nonaddictive Opioid Alternative. *J. Med. Chem.* **2021**, *64*, 1856–1872.

[28] Mashayekhi, M.; Wanjalla, C. N.; Warren, C. M.; Simmons, J. D.; Ghoshal, K.; Pilkinton, M.; Bailin, S. S.; Gabriel, C. L.; Pozzi, A.; Koethe, J. R.; et al. The soluble epoxide hydrolase inhibitor GSK2256294 decreases the proportion of adipose pro-inflammatory T cells. *Prostaglandins Other Lipid Mediat.* **2022**, *158*, 106604.

[29] Capan, I.; Jordan, P. M.; Olgac, A.; Caliskan, B.; Kretzer, C.; Werz, O.; Banoglu, E. Discovery and Optimization of piperazine urea derivatives as soluble epoxide hydrolase (sEH) inhibitors. *ChemMedChem.* **2022**, *17*, e202200137.

[30] Gur Maz, T.; Koc, B.; Jordan, P. M.; Ibis, K.; Caliskan, B.; Werz, O.; Banoglu, E. Benzoxazolone-5-urea derivatives as human soluble epoxide hydrolase (sEH) inhibitors. *ACS Omega.* **2023**, *8*, 2445–2454.

[31] Lengerli, D.; Bakht, A.; Caliskan, K.; Dahlke, P.; Bal, N. B.; Jordan, P. M.; Caliskan, B.; Werz, O.; Banoglu, E. Phenyl-benzyl-ureas with pyridazinone motif: Potent soluble epoxide hydrolase inhibitors with enhanced pharmacokinetics and efficacy in a paclitaxel-induced neuropathic pain model. *Eur. J. Med. Chem.* **2025**, *290*, 117510.

[32] Lengerli, D.; Koç, B.; Jordan, P. M.; Çalışkan, K.; Çalışkan, B.; Werz, O.; Banoglu, E. Potent soluble epoxide hydrolase inhibitors based on thiazole-5-carboxamide structure with imidazolidinone moiety as a secondary pharmacophore. *Bioorg. Chem.* **2025**, *163*, 108644.

[33] Turanli, S.; Ergul, A. G.; Jordan, P. M.; Olgac, A.; Caliskan, B.; Werz, O.; Banoglu, E. Quinazoline-4(3H)-one-7-carboxamide derivatives as human soluble epoxide hydrolase inhibitors with developable 5-lipoxygenase activating protein inhibition. *ACS Omega.* **2022**, *7*, 36354–36365.

[34] Eldrup, A. B.; Soleymanzadeh, F.; Farrow, N. A.; Kukulka, A.; De Lombaert, S. Optimization of piperidyl-ureas as inhibitors of soluble epoxide hydrolase. *Bioorg. Med. Chem. Lett.* **2010**, *20*, 571–575.

[35] Li, F.; Zhu, W. F.; Empel, C.; Datsenko, O.; Kumar, A.; Xu, Y. M.; Ehrler, J. H. M.; Atodiresei, I.; Knapp, S.; Mykhailiuk, P. K.; et al. Photosensitization enables Pauson-Khand-type reactions with nitrenes. *Science* **2024**, *383*, 498–503.

[36] Wixtrom, R. N.; Silva, M. H.; Hammock, B. D. Affinity purification of cytosolic epoxide hydrolase using derivatized epoxy-activated sepharose gels. *Anal. Biochem.* **1988**, *169*, 71–80.

[37] Waltenberger, B.; Garscha, U.; Temml, V.; Liers, J.; Werz, O.; Schuster, D.; Stuppner, H. discovery of potent soluble epoxide hydrolase (sEH) inhibitors by pharmacophore-based virtual screening. *J. Chem. Inf. Model.* **2016**, *56*, 747–762.

[38] Hu, E.; Kunz, R. K.; Chen, N.; Rumfelt, S.; Siegmund, A.; Andrews, K.; Chmait, S.; Zhao, S.; Davis, C.; Chen, H.; et al. Design, optimization, and biological evaluation of novel keto-benzimidazoles as potent and selective inhibitors of phosphodiesterase 10A (PDE10A). *J. Med. Chem.* **2013**, *56*, 8781–8792.